study of osteoinduction in hydroxyapatite-derived biomaterials in an adult sheep model. II. Bioengineering implants to optimize bone replacement in reconstruction of cranial defects. Plast Reconstr Surg 2004;114:1155–1163.

41. Fujibayashi S, Neo M, Kim HM, Kokubo T, Nakamura T. Osteoinduction of bioactive titanium metal. Key Eng Mater 2004;254/252:953–956.
42. Li XM, Feng QL, Cui FZ. In vitro degradation of porous nano-hydroxyapatite/collagen/PLLA scaffold reinforced by chitin fibres. Mater Sci Eng C 2006;26:716–720.
43. Yuan H, de Bruijn JD, Zhang X. Osteoinduction by porous alumina ceramic. European Conference on Biomaterials. London; 2001. p 209.
44. Fujibayashi S, Neo M, Kim HM, Kokubo T, Nakamura T. Osteoinduction of porous bioactive titanium metal. Biomaterials 2004;25:443–450.
45. Li Y, Lee IS, Cui FZ, Choi SH. The biocompatibility of nanostructured calcium phosphate coated on micro-arc oxidized titanium. Biomaterials 2008;29:2025–2032.
46. Li XM, Van Blitterswijk CA, Feng QL, Cui FZ, Watari F. The effect of calcium phosphate microstructure on bone-related cells in vitro. Biomaterials 2008;29:3306–3316.
47. Popat KC, Chatvanichkul KI, Barnes GL, Latempa TJ, Grimes CA, Desai TA. Osteogenic differentiation of marrow stromal cells cultured on nanoporous alumina surfaces. J Biomed Mater Res A 2007;80:955–964.
48. Yim EKF, Pang SW, Leong KW. Synthetic nanostructures inducing differentiation of human mesenchymal stem cells into neuronal lineage. Exp Cell Res 2007;313:1820–1829.
49. Ratner BD, Johnston AB, Lenk TS. Biomaterials surfaces. J Biomed Mater Res A 1987;21:59–90.
50. Zreiqat H, Standard OC, Gengenbach T, Steele J, Howlett CR. The role of surface characteristics in the initial adhesion of human bone-derived cells on ceramics. Cell Mater 1996;6:45–56.
51. Abrams GA, Goodman SL, Nealey PF, Franco M, Murphy CJ. Nanoscale topography of the basement membrane underlying the corneal epithelium of the rhesus macaque. Cell Tissue Res 2000;299:39–46.
52. Kumazawa R, Watari F, Takashi N, Tanimura Y, Uo M, Totsuka Y. Effects of Ti ions and particles on neutrophil function and morphology. Biomaterials 2002;23:3757–3764.
53. Aoki N, Akasaka T, Watari F, Yokoyama A. Carbon nanotubes as scaffolds for cell culture and effect on cellular functions. Dental Mater J 2007;26:178–185.
54. Kilpadi KL, Sawyer AA, Prince CW, Chang PL, Bellis SL. Primary human marrow stromal cells and SaOs-2 osteosarcoma cells use different mechanisms to adhere to hydroxylapatite. J Biomed Mater Res A 2003;68:273–285.
55. Habibovic P, Yuan HP, Van den Doel M, Sees TM, Van Blitterswiik CA, De Groot K. Relevance of osteoinductive biomaterials in critical-sized orthotopic defect. J Orthop Res 2006; 24:867–876.
56. Kondo N, Ogose A, Tokunaga K, Umezu H, Arai K, Kudo N, Hoshino M, Inoue H, Irie H, Kuroda K, Mera H, Endo N. Osteoinduction with highly purified beta-tricalcium phosphate in dog dorsal muscles and the proliferation of osteoclasts before heterotopic bone formation. Biomaterials 2006; 27:4419–4427.
57. Yamasaki H, Sakai H. osteogenic response to porous hydroxyapatite ceramics under the skin of dogs. Biomaterials 1992;13:308–312.
58. Ripamonti U, Van den Heever B, Van Wyk J. Expression of the osteogenic phenotype in porous hydroxyapatite implanted extraskeletally in baboons. Matrix 1993;13:491–502.
59. Magan A, Ripamonti U. Geometry of porous hydroxyapatite implants influences osteogenesis in baboons (*Papio Ursinus*). J Craniofac Surg 1996;7:71–78.
60. Hing KA. Bioceramic bone graft substitutes: Influence of porosity and chemistry. Int J Appl Ceram Tech 2005;2:184–199.

IOP PUBLISHING BIOMEDICAL MATERIALS

Biomed. Mater. 4 (2009) 015005 (8pp) doi:10.1088/1748-6041/4/1/015005

Maturation of osteoblast-like SaoS2 induced by carbon nanotubes

Xiaoming Li[1,5], Hong Gao[2], Motohiro Uo[1], Yoshinori Sato[3], Tsukasa Akasaka[1], Shigeaki Abe[1], Qingling Feng[4], Fuzhai Cui[4] and Fumio Watari[1]

[1] Department of Biomedical Materials and Engineering, Graduate School of Dental Medicine, Hokkaido University, Kita Ku Kita 13, Nishi 7, Sapporo 060-8586, Japan
[2] Division of Applied Bioscience, Graduate School of Agriculture, Hokkaido University, Sapporo 060-8586, Japan
[3] Graduate School of Environmental Studies, Tohoku University, Sendai, Japan
[4] Key Laboratory of Advanced Materials, Department of Materials Science and Engineering, Tsinghua University, Beijing 100084, People's Republic of China

E-mail: x.m.li@hotmail.com

Received 7 July 2008
Accepted for publication 27 August 2008
Published 4 November 2008
Online at stacks.iop.org/BMM/4/015005

Abstract

Osteogenic maturation of the osteoblast is crucial for bone formation. In this study, multi-walled carbon nanotubes (MWCNTs) and graphite (GP) were pressed as compacts. The greater ability of carbon nanotubes to adsorb proteins, compared with graphite, was shown. Human osteoblast-like SaoS2 cells were cultured and the cell response to the two kinds of compacts was compared *in vitro*. Meanwhile, we used cell culture on the culture plate as a control. Assays for osteonectin, osteopontin and osteocalcin gene expression, total protein (TP) amount, alkaline phosphatase activity (ALP) and DNA of cells cultured on the samples were done. During the conventional culture, significantly higher osteonectin, osteopontin and osteocalcin gene expression level, ALP/DNA and TP/DNA on carbon nanotubes were found. To confirm the hypothesis that the larger amount of specific proteins adsorbed on the carbon nanotubes was crucial for this, the compacts were pre-soaked in culture medium having additional recombinant human bone morphogenetic protein-2 (rhBMP-2) before cell culture. Compared with GP, osteonectin, osteopontin and osteocalcin gene expression level, ALP/DNA and TP/DNA of the cells tested increased more on the MWCNTs after the compacts were pre-soaked in the culture medium with rhBMP-2. The results indicated that the carbon nanotubes might induce osteogenic maturation of the osteoblast by adsorbing more specific proteins.

Introduction

A scaffold is one of the key components in the tissue engineering paradigm in which it can function as a template to allow new tissue growth and also provide temporary structural support while serving as a delivery vehicle for cells and/or bioactive molecules [1–7]. Since nanotechnology embraces a system whose core of materials is in the range of nanometers (10^{-9} m), there are many similarities between nanophase materials and components of biological organs [8–10]. So, nanomaterials should logically have a significant impact on tissue engineering [11–14].

Carbon nanotubes (CNTs), one of the most representative nanomaterials, possess exceptional mechanical, thermal and electrical properties, facilitating their use as reinforcements or additives in various materials, such as plastics, metals and ceramics, to improve properties of the materials and introduce novel functionalities [15]. At present, carbon nanotubes have been extensively studied for use in biomaterial applications, and biomaterials using CNTs are expected to be developed for clinical use [14–27]. A lot of studies have been

[5] Corresponding author.

carried out on the interaction between CNTs and a variety of cells including osteoblasts, showing CNTs to be excellent substrates for cellular attachment and growth [28–36]. But few (if any) studies have elucidated the effect of CNTs on the differentiation and maturation of the attached cells, although these processes are even more important for tissue repair [37–39].

It has been suggested that nanostructures of the biomaterials are critical to start the differentiation of cells [2, 40–43]. In other words, the microenvironment around the cells may be crucial [2]. Park *et al* suggested that nanostructured Ca coating of Ti surfaces may be used as a potentially effective method for enhancing the osseointegration of the implants, by accelerating the proliferation and differentiation of osteoblast cells on their surfaces in the early bone healing phase [41]. Popat *et al* presented osteogenic differentiation of C57 BJ mice marrow stromal cells on nanoporous alumina surfaces, suggesting the ability of nanostructured biomaterials to enhance cell differentiation [44]. Yim *et al* reported that the nanopatterns, reproduced on poly(dimethylsiloxane) (PDMS) using soft lithography on the nanoimprinted poly(methyl methacrylate) (PMMA)-coated Si master mold, played an important role in directing differentiation of adult stem cells into neuronal lineage [45]. Ou *et al* reported that formation of nanohydrides by cathodization and oxidation by anodization are believed to promote biocompatibility and improve the bone-to-interface contact, accelerating initial osseointegration and re-osseointegration [46].

In this study, multi-walled carbon nanotubes (MWCNTs) and graphite (GP) were pressed as compacts. Human osteoblast SaoS2 cells were cultured on the two kinds of compacts with and without adsorbing recombinant human bone morphogenetic protein-2 (rhBMP-2). The cell differentiation and osteogenic maturation on the two kinds of compacts were respectively compared *in vitro*. Meanwhile, we used cell culture on the culture plate as a control.

Materials and methods

Materials

MWCNTs used in this study were obtained from NanoLab (Brighton, MA, USA). The MWCNTs of a curled shape and about 90 nm in diameter were produced by the chemical vapor deposition (CVD) method. The raw MWCNTs were refluxed in a hydrochloric solution and then washed thoroughly with deionized water and completely dried. The GP particles used in this study were about 4.5 μm in diameter.

Fabrication of compacts

MWCNTs and GP were separately compacted serially in a steel-tool die via a uniaxial pressing cycle (0.09 GPa for 2 min, then 0.22 GPa for 3 min and finally 0.36 GPa for 3 min) at room temperature. The compacts were washed ultrasonically with acetone, 70% ethanol and deionized water for 15 min and were then dried at 60 °C. All the compacts were sterilized by ultraviolet radiation for 48 h prior to experiments with cells. The morphology of the compacts was examined by scanning electron microscopy (SEM; S-4000, Hitachi, Japan).

Evaluation of protein adsorption on the compacts

Before cell culture, the ability of protein adsorption of the compacts was evaluated. At first, 0.25% fetal bovine serum (FBS; Biowest) (250 μl FBS in a 100 ml 25 ppm NaN_3 solution) was sterilized with a 0.22 μm filter. After immersing the compacts respectively for 1, 4 and 7 days, the remaining protein content per cent (P_l) of the FBS solution (3 ml per sample, $n = 5$) was measured with the QuantiPro™ bicinchoninic acid (BCA) assay kit (TaKaRa Bio Inc, Japan), according to the guideline of the company. The adsorbed protein (P_a) was determined from the formula $(0.25\% - P_l)/0.25\%$.

Conventional cell culture on the samples

The compacts were placed in the cell culture plates. Then SaoS2 cells were respectively seeded on the compacts with a cell density of 3.0×10^4 per sample. The samples were then put into an incubator at 37 °C in a humidified atmosphere with 5% CO_2 and 95% air for 4 h. Finally, 2.5 ml culture medium, Dulbecco's modified Eagle's medium (DMEM; Sigma) with 10% FBS and 1% penicillin/streptomycin (100 U ml^{-1} penicillin, 10 μg ml^{-1} streptomycin), was added to the wells of the plates and then the plates were put back in the incubator. The culture media were refreshed twice a week.

DNA, alkaline phosphatase (ALP) and total protein (TP) analyses

After cell culture, the samples with cells were washed by phosphate buffered saline (PBS) three times after the cultured medium was totally removed. Then the samples were stored in the freezer at −80 °C for at least 12 h for the biochemical analyses. As soon as the plates were taken out of the freezer, they were kept on ice, prepared in advance. Then 0.5 ml 0.2% triton was put into each well with samples in the plates. The plates were shaken gently for 45 min. Finally, the triton solutions with lysed cells were analyzed for DNA, ALP and protein content.

The DNA content was measured with the CyQuant Cell Proliferation Assay Kit (Invitrogen), according to the guideline of the company. 0.1 ml of each sample ($n = 4$) was diluted in the lysis buffer, which was included in the kit, to a final volume of 1.0 ml test tubes. Then 1.0 ml of an aqueous working solution (dye) was added to each sample. After the tubes were incubated for about 3 min, the fluorescence using instrument parameters was measured at an emission wavelength of 520 nm and an excitation of 480 nm. The DNA content of cells attached to the porous samples was counted through a pre-made standard DNA curve. The DNA content was expressed as mean ± SD.

For the determination of the ALP content, 20 μl of each sample ($n = 4$) was added to the wells of a 96-well plate and then a 100 μl paranitrophenylphosphate (PNP) solution was added. After being shaken gently, the plate was incubated at

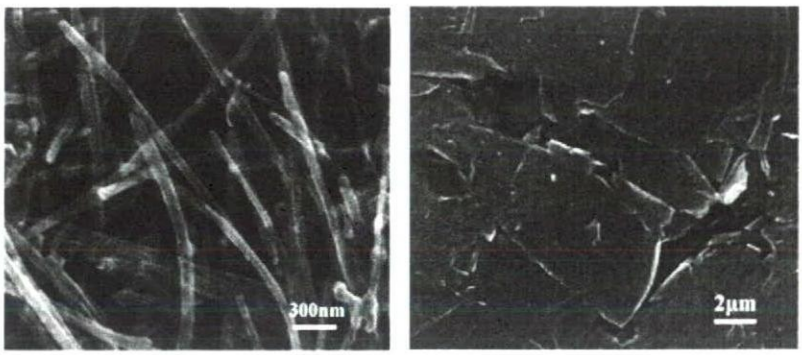

(a) (b)

Figure 1. SEM images of the compacts: MWCNTs (*a*) and GP (*b*).

37 °C for 15 min. After an 80 μl stop solution (0.2 mol l^{-1} sodium hydroxide) was added, the plate was read with a BIO-TEK automatic microplate reader at 405 nm. For the standard curve, serial dilutions of p-nitrophenol were made. Finally, the ALP content of cells was counted through the standard curve. The value was expressed as mean ± SD.

For the determination of the protein content, 100 μl of each sample ($n = 4$) was added to the wells of a 96-well plate and then a 100 μl BCA solution was added. Then, the plate was continuously shaken for 2 h in the dark at room temperature. Finally, the protein content was measured with the QuantiPro™ BCA Assay Kit (TaKaRa Bio Inc, Japan), according to the guideline of the company. The protein content, expressed as mean ± SD, was counted through a pre-made standard protein curve.

Osteonectin, osteopontin and osteocalcin gene expression

Cell lysate was collected after week 1, and the total RNA was isolated and purified with RNeasy columns (Qiagen, Basel). The isolated RNA was reverse-transcripted to cDNA with the StratScript enzyme (Stratagene, San Diego, CA). Quantitative real-time RT-PCR (Taq Man ABI Prism 7700, Applied Biosystem, Foster City, CA) was used to measure the gene expression of osteonectin, osteopontin, osteocalcin and a housekeeping gene (18S) using the amplifluor universal detection system (Intergen, Purchase, NY). Primers were designed with the Software Primer Expresst (Applied Biosystem). Primers were purchased from Integrated DNA Technologies (Coralville, IA). Use of 18S allowed the different samples to be normalized and compared between experiments.

Cell culture on the samples after adsorbing rhBMP-2

At first, the samples were respectively immersed in rhBMP-2 (Yamanouchi Pharmaceutical Co. Ltd., Tokyo, Japan) solutions (rhBMP-2 in the cell culture medium) with a concentration of 500 ng ml^{-1} for 24 h in an incubator at 37 °C in a humidified atmosphere with 5% CO_2 and 95% air. Then, the solution was completely removed and the samples were washed by the cultured medium of SaoS2 with 1% FBS three times. And then, the cells were respectively cultured on the samples with a cell density of 5.0×10^4 per sample. After cell culture in the culture medium with 1% FBS for a certain time, DNA, ALP and the total protein content were examined with the methods mentioned above.

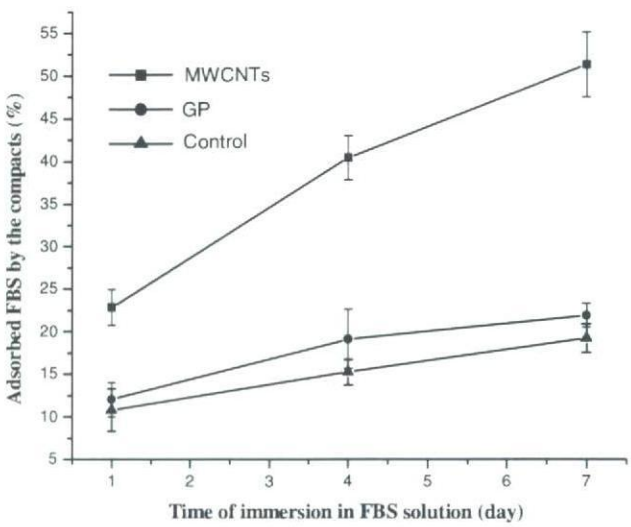

Figure 2. Ability to adsorb proteins of the samples ($n = 5$).

Statistical analysis

Data obtained were statistically analyzed with one-way analysis of variance (ANOVA), followed by Tukey's post-hoc test (SPSS Inc., Chicago, IL, USA). $P < 0.05$ was regarded as significant difference.

Results

Figure 1 shows the SEM images of the compacts. The distinct difference in the structures of the MWCNTs and GP compacts was exhibited. MWCNTs formed a packed meshwork nanostructure, while GP compacts were formed with particles of about 4.5 μm. The ability of protein adsorption of the compacts is shown in figure 2, which shows that MWCNT compacts had much greater ability to adsorb protein than GP compacts. Although the mean value of the protein adsorption of GP compacts was higher than that of

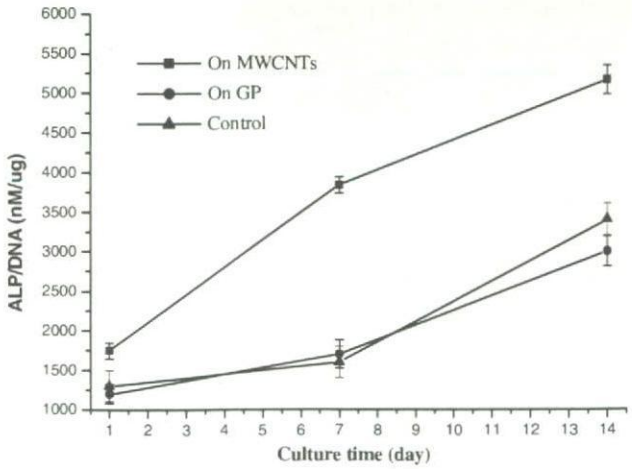

Figure 3. ALP/DNA of the SaoS2 cells conventionally cultured on samples ($n = 4$).

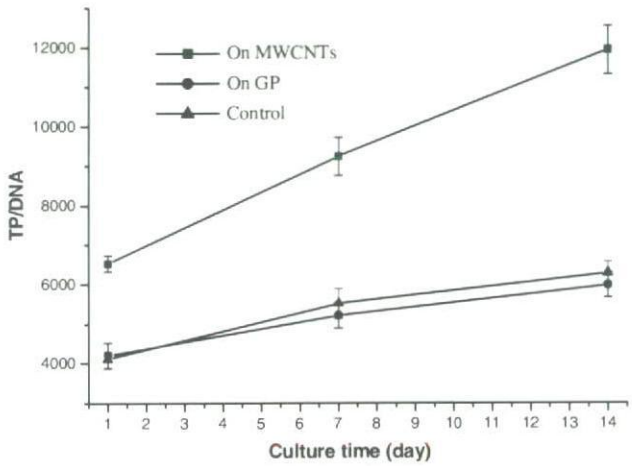

Figure 4. Protein/DNA of the SaoS2 cells conventionally cultured on samples ($n = 4$).

the culture plates (control), the statistical analysis showed that there was no significant difference between the two group values ($P > 0.05$).

Figure 3 shows the results of ALP/DNA (alkaline phosphatase per unit cell). ALP/DNA of the SaoS2 cells cultured on MWCNT compacts was significantly higher than that on GP compacts and on the plates at each culture time point of 1, 7 and 14 days, whereas this value for GP compacts and the control had no significant difference at each time point.

TP/DNA (total protein content per unit cell) is shown in figure 4. TP/DNA of the SaoS2 cells on MWCNTs was significantly higher than on GP and the culture plates at each culture time point of 1, 7 and 14 days. At day 14, the value for MWCNTs was about twice the value for GP. Although the mean value for GP compacts was higher than that for the control at days 7 and 14, the statistical analysis showed that there was no significant difference between the two group values ($P > 0.05$).

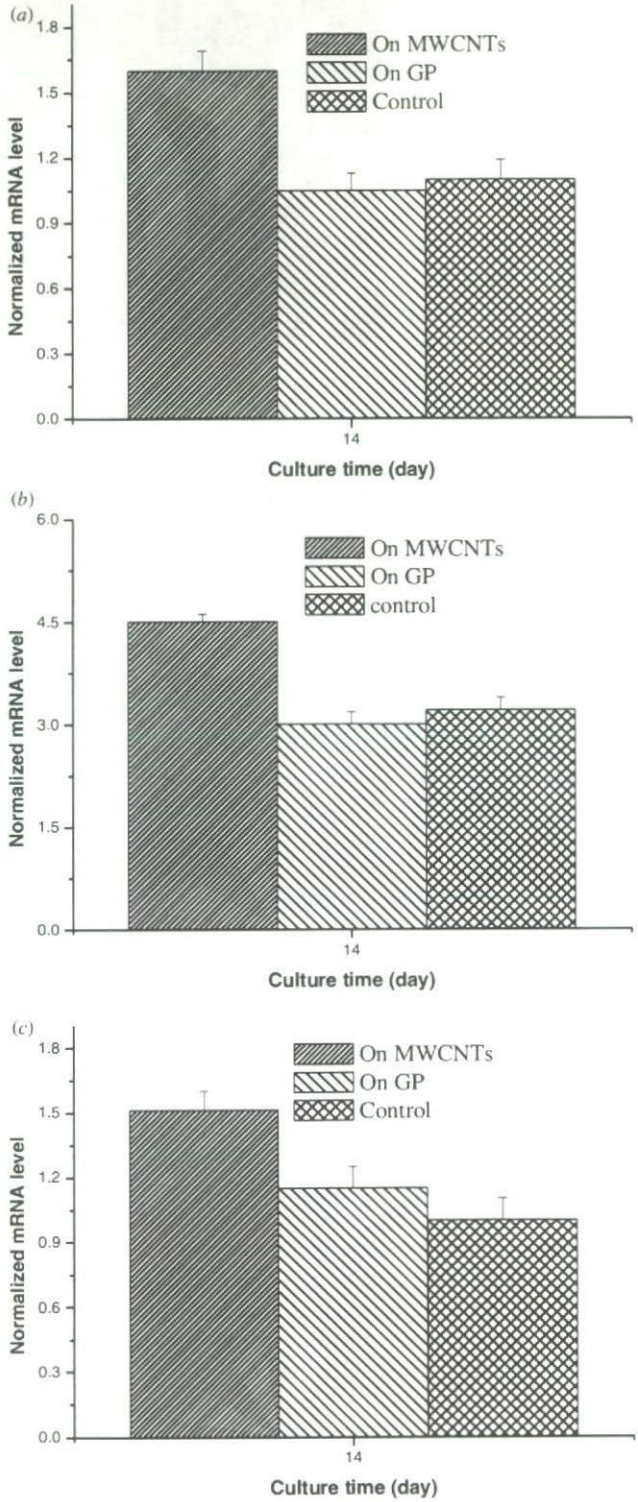

Figure 5. Gene expression of (*a*) osteonectin, (*b*) osteocalcin and (*c*) osteopontin normalized by the gene expression of 18S of cells conventionally cultured on different samples ($n = 4$).

As is shown in figure 5, statistically higher osteonectin, osteopontin and osteocalcin gene expression of SaoS2 at day 14 on MWCNTs than on GP scaffolds was found ($P < 0.05$). There was no significant difference in the osteonectin,

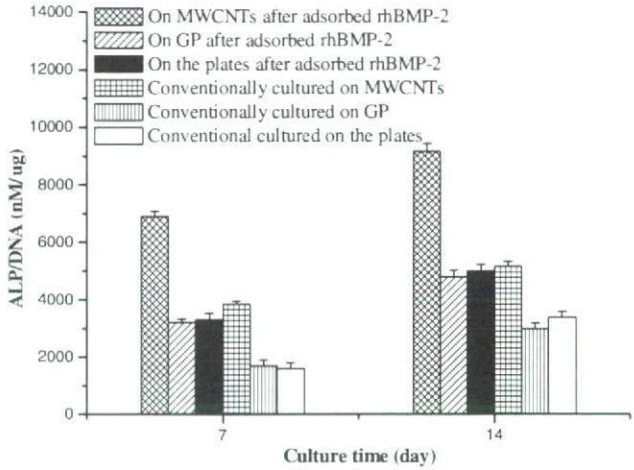

Figure 6. ALP/DNA of the SaoS2 cells cultured on samples with and without the adsorption of rhBMP-2 in advance ($n = 4$).

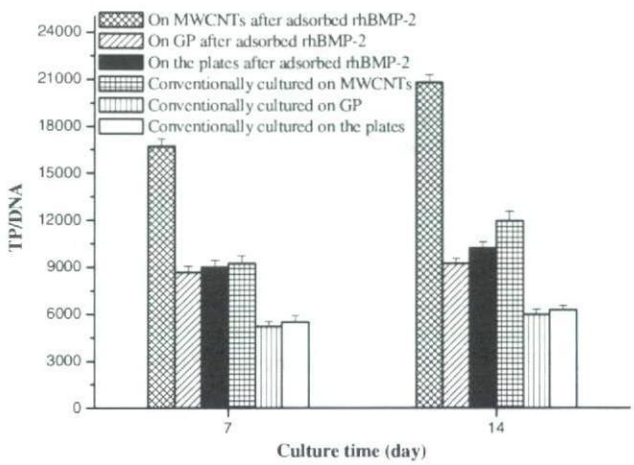

Figure 7. Total-protein/DNA of the SaoS2 cells cultured on samples with and without the adsorption of rhBMP-2 in advance ($n = 4$).

osteopontin and osteocalcin gene expression of SaoS2 at day 14 between GP and control ($P > 0.05$).

Figure 6 shows ALP/DNA of the SaoS2 cells on the samples after adsorbing rhBMP-2 at day 7 and day 14, compared with the results of the conventional cell culture. ALP/DNA of the cells on all the samples increased after the adsorption of rhBMP-2. But the value for MWCNTs increased most significantly. The value for GP and the control had no significant difference even after the adsorption of rhBMP-2 ($P > 0.05$).

TP/DNA of the SaoS2 cells on the samples after adsorbing rhBMP-2 at day 7 and day 14, compared with the results of the conventional cell culture, is shown in figure 7. The TP/DNA of cells on all the samples all increased after the adsorption of rhBMP-2. But the value for MWCNTs increased most observably. The value for GP and the culture plates had no significant difference even after the adsorption of rhBMP-2 ($P > 0.05$).

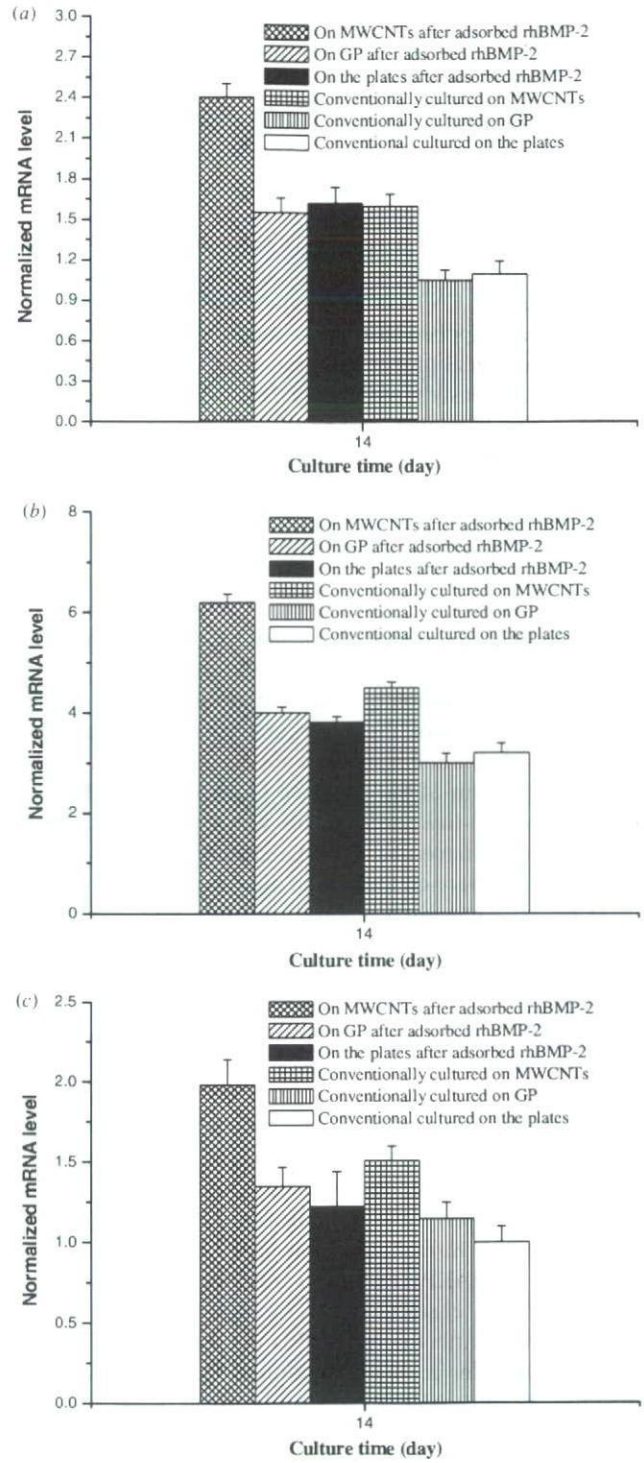

Figure 8. Gene expression of (*a*) osteonectin, (*b*) osteocalcin and (*c*) osteopontin normalized by the gene expression of 18S of cells cultured on the different samples with and without the adsorption of rhBMP-2 in advance ($n = 4$).

Figure 8 shows osteonectin, osteopontin and osteocalcin gene expression of the SaoS2 cells on the samples after adsorbing rhBMP-2 at day 14, compared with the results of the conventional cell culture. Osteonectin, osteopontin and

osteocalcin gene expression of the cells on all the samples all increased after the adsorption of rhBMP-2. But the value for MWCNTs increased most significantly. The value for GP and the control had no significant difference even after the adsorption of rhBMP-2 ($P > 0.05$).

Discussion

Because CNTs have a high elastic modulus, approaching 1 TPa, and exceptional tensile strengths, ranging from 20 to 100 GPa, use of CNTs in the biomaterials, such as ceramics and polymers, applied to bone is anticipated to improve the overall mechanical properties for applications, such as high-strength arthroplasty prostheses that are expected to remain in the body for a long time or fixation plates and screws that will not fail or impede the healing of bone [15]. In these cases, the effect of CNTs on the performance of osteoblasts seems most important.

It has been indicated that the biological response of cells to implanted material is determined not only by its chemistry, but also by structure [2, 47, 48]. The nano-dimensionality of nature has logically suggested that nanostructured biomaterials should have a positive effect on the cell functions [49, 50].

Both carbon nanotubes and GP are isomorphs of pure carbon, composed of the same grapheme sheet structure. However, only carbon nanotubes are nano-scaled. So in this study, comparison of the influence of carbon nanotubes and GP on osteoblast-like SaoS2 *in vitro* was done to figure out the effect of carbon nanotubes on cellular functions. Meanwhile, we used cell culture on the culture plate as a control.

Cell differentiation should be the most important evaluation point for biomaterials because it may directly contribute to the tissue repair. The satisfactory differentiation and maturation of osteoblasts are essential for bone tissue regeneration. So in this study, our focus has been on the effect of carbon nanotubes on the maturation of the cultured osteoblasts. This may be the first time that the effect of carbon nanotubes on the osteogenic maturation, especially the osteoblastic gene expression of osteoblasts, was researched.

ALP, a noncollagenous protein, is a highly specific marker of bone formation, osteoblast function and a significant predictor of the formation of osteogenic cells [51]. In this study, we used ALP/DNA to express the ALP activity per cell, thereby to characterize the ability of bone formation of each cell. Furthermore, ALP is one kind of protein and only accounts for a small proportion of the total proteins in cells. Besides ALP, there may be some others proteins, which may be the markers of the formation of osteogenic cells [52]. Evaluating TP in cells may be an effective method for evaluating the potential differentiation of cells. So, in our study, TP/DNA was used as an additional marker of the activity per unit cell for the potential cell differentiation.

Osteocalcin, osteopontin and osteonectin are important osteoblastic markers and are expressed at different maturation stages of the osteoblasts [53]. These three genes have been shown to be differently involved in the bone mineralization process. Osteocalcin, which is the most osteoblast-specific gene yet known [54], has been demonstrated to stimulate bone mineral maturation [55]. Osteopontin has been shown to inhibit the crystal growth of hydroxyapatite, e.g. [56], while osteonectin has been suggested to promote collagen mineralization [57].

From the results of conventional cell culture, we found that the ALP/DNA of SaoS2 cells on MWCNTs was significantly higher than on GP and the culture plates, suggesting that MWCNTs induce this kind of cell to differentiate into osteogenetic cells more than GP and culture plates. TP/DNA of the cells on MWCNTs was significantly higher than on GP and the culture plates, which might suggest that MWCNTs induce the potential differentiation of cells more than GP and culture plates. In other words, cells cultured on MWCNTs were more active. Moreover, the higher osteonectin, osteopontin and osteocalcin gene expression of SaoS2 at 7 days on MWCNT than on GP scaffolds suggests that the MWCNT scaffolds could provide a better environment for the mineralization process and the osteoblastic maturation.

Some publications have shown that, although some materials had the same chemical composition, they had different effects on the cell differentiation [2, 58–60]. These materials, with specific structures, indicating a larger surface area and therefore greater ability to adsorb proteins, have been shown to induce cell differentiation. The work of Ripamonti and co-workers demonstrated that bone formation in hydroxyapatite was linked to the precise shape of surface concavities in implants, which indicated a larger surface area; by using immunolocalization, they demonstrated that the bone formation occurred as a result of a concentration of specific proteins within the surface concavities [61, 62].

Why did the MWCNT scaffolds induce the maturation of the SaoS2 cells in this study? Since the MWCNT scaffolds had much greater ability to adsorb protein (figure 2), we hypothesized that the large amount of proteins adsorbed on MWCNTs played an important role in inducing cellular functions.

To confirm this hypothesis, we immersed the samples in the culture medium containing rhBMP-2 to make them adsorb more proteins before cell culture. The results showed that after the adsorption of rhBMP-2, both TP/DNA and ALP/DNA increased on all samples. Impressively, the value for MWCNTs increased most significantly. The increments of TP/DNA and ALP/DNA for MWCNTs were respectively about 11 times and 18 times those for GP and the control at both day 4 and day 7. Therefore, the results of cell culture after the adsorption of rhBMP-2 might be an effective proof for our hypothesis.

Hing [63] has reported that competitive protein adsorption at a bioactive surface may vary in three ways, which is the quantity of protein adsorbed, the species of protein adsorbed and the confirmation of the adsorbed protein. Also, he supposed that nanostructures might thus influence protein adsorption by providing a larger surface area, thereby increasing the quantity of adsorbed growth factors above a critical level for cell recruitment and activation. In our study, we substantiated the importance of the protein adsorption. Carbon nanotubes might adsorb a large number of proteins due to their larger surface area and unique electronic, catalytic

and chemical properties. These proteins might be helpful for the cell differentiation and maturation of the osteoblasts and therefore directly contribute to bone tissue repair. Since *in vivo* cellular microenvironments are immobilized within tissue, and consist of diverse extracellular matrix proteins, CNTs might induce cellular functions *in vivo* by adsorbing a large number of proteins.

Conclusion

Carbon nanotubes might induce the osteoblastic differentiation and osteogenic maturation of the cultured human osteoblast-like cells (SaoS2) by adsorbing a large number of proteins, which indicated that carbon nanotubes might be a candidate scaffold material for bone tissue engineering.

Acknowledgment

This study was financially supported by JSPS (Japan Society for the Promotion of Science).

References

[1] Li X M, Feng Q L, Liu X H, Dong W and Cui F Z 2006 Collagen-based implants reinforced by chitin fibres in a goat shank bone defect model *Biomaterials* **27** 1917–23

[2] Li X M, Van Blitterswijk C A, Feng Q L, Cui F Z and Watari F 2008 The effect of calcium phosphate microstructure on bone-related cells *in vitro Biomaterials* **29** 3306–16

[3] Capito R M and Spector M 2007 Collagen scaffolds for nonviral IGF-1 gene delivery in articular cartilage tissue engineering *Gene Therapy* **14** 721–32

[4] Spector M 2006 Biomaterials-based tissue engineering and regenerative medicine solutions to musculoskeletal problems *Swiss Med. Wkly* **136** 293–301

[5] Li X M, Feng Q L, Wang W J and Cui F Z 2006 Chemical characteristics and cytocompatibility of collagen-based scaffold reinforced by chitin fibers for bone tissue engineering *J. Biomed. Mater. Res.* **77B** 219–26

[6] Li X M, Gao H, Uo M, Sato Y, Akasaka T, Feng Q L, Cui F Z, Liu X H and Watari F 2008 Effect of carbon nanotubes on cellular functions in vitro *J. Biomed. Mater. Res.* A (DOI: 10.1002/jbm.a.32203)

[7] Li X M, Feng Q L, Jiao Y F and Cui F Z 2005 Collagen-based scaffolds reinforced by chitosan fibres for bone tissue engineering *Polym. Int.* **54** 1034–40

[8] Venugopal J, Low S, Choon A T and Ramakrishna S 2008 Interaction of cells and nanofiber scaffolds in tissue engineering *J. Biomed. Mater. Res.* **84B** 34–48

[9] Labhasetwar V 2005 What is next for nanotechnology? *J. Biomed. Nanotechnol.* **1** 373–4

[10] Webster T J, Hellenmeyer E L and Price R L 2005 Increased osteoblast functions on theta plus delta nanofiber alumina *Biomaterials* **26** 953–60

[11] Watari F *et al* 2008 Behavior of *in vitro*, *in vivo* and internal motion of micro/nano particles of titanium, titanium oxides and others *J. Ceram. Soc. Japan* **116** 1–5

[12] Watari F, Yokoyama A, Omori M, Hirai T, Kondo H, Uo M and Kawasaki T 2004 Biocompatibility of materials and development to functionally graded implant for bio-medical application *Compos. Sci. Technol.* **64** 893–908

[13] Yokoyama A *et al* 2005 Biological behavior of hat-stacked carbon nanofibers in the subcutaneous tissue in rats *Nano. Lett.* **5** 157–61

[14] Harrison B S and Atala A 2007 Carbon nanotube applications for tissue engineering *Biomaterials* **28** 344–53

[15] Usui Y *et al* 2008 Carbon nanotubes with high bone-tissue compatibility and bone-formation acceleration effects *Small* **4** 240–6

[16] Firkowska I, Olek M, Pazos-Perez N, Rojas-Chapana J and Giersig M 2006 Highly ordered MWNT-based matrixes: topography at the nanoscale conceived for tissue engineering *Langmuir* **22** 5427–34

[17] Aoki N, Yokoyama A, Nodasaka Y, Akasaka T, Uo M, Sato Y, Tohji K and Watari F 2006 Strikingly extended morphology of cells grown on carbon nanotubes *Chem. Lett.* **35** 508–9

[18] Correa-Duarte M A, Wagner N, Rojas-Chapana J, Morsczeck C, Thie M and Giersig M 2004 Fabrication and biocompatibility of carbon nanotube-based 3D networks as scaffolds for cell seeding and growth *Nano Lett.* **4** 2233–6

[19] Uo M, Tamura K, Sato Y, Yokoyama A, Watari F, Totsuka Y and Tohji K 2005 The cytotoxicity of metal-encapsulating carbon nanocapsules *Small* **1** 816–9

[20] Akasaka T and Watari F 2005 Nano-architecture on carbon nanotube surface by biomimetic coating *Chem. Lett.* **34** 826–7

[21] MacDonald R A, Laurenzi B F, Viswanathan G, Ajayan P M and Stegeman J P 2005 Collagen-carbon nanotube composite materials as scaffolds in tissue engineering *J. Biomed. Mater. Res.* **74A** 489–96

[22] Kam N W S, Jessop T C, Wender P A and Dai H 2004 Nanotube molecular transporters: internalization of carbon nanotube–protein conjugates into mammalian cells *J. Am. Chem. Soc.* **126** 6850–1

[23] Kam N W S, Liu Z and Dai H 2005 Functionalization of carbon nanotubes via cleavable disulfide bonds for efficient intracellular delivery of siRNA and potent gene silencing *J. Am. Chem. Soc.* **127** 12492–3

[24] Supronowicz P R, Ajayan P M, Ullmann K R, Arulanandam B P, Metzger D W and Bizios R 2002 Novel current-conducting composite substrates for exposing osteoblasts to alternating current stimulation *J. Biomed. Mater. Res.* **59** 499–506

[25] Chen R L, Bangsaruntip S, Drouvalakis K A, Kam N W S, Shim M and Li Y 2003 Noncovalent functionalization of carbon nanotubes for highly specific electronic biosensors *Proc. Natl Acad. Sci.* **100** 4984–9

[26] Kiura K, Sato Y, Yasuda M, Fugetsu B, Watari F, Tohji K and Shibata K 2005 Activation of human monocytes and mouse splenocytes by single-walled carbon nanotubes *J. Biomed. Nanotechnol.* **1** 359–64

[27] Sato Y *et al* 2005 Influence of length on cytotoxicity of multi-walled carbon nanotubes against human acute monocytic leukemia cell line THP-I *in vitro* and subcutaneous tissue of rats *in vivo Mol. Biosyst.* **1** 176–82

[28] Pantarotto D, Briand J, Prato M and Pianco A 2004 Translocation of bioactive peptides across cell membranes by carbon nanotubes *Chem. Commun.* **10** 16–7

[29] Mwenifumbo S, Shaffer M S and Stevens M M 2007 Exploring cellular behaviour with multi-walled carbon nanotube constructs *J. Mater. Chem.* **17** 1894–902

[30] Lu Q, Moore J M, Huang G, Mount A S, Rao A M and Larcom L L 2004 RNA polymer translocation with single-walled carbon nanotubes *Nano Lett.* **4** 2473–77

[31] Cherukuri P, Bachilo S M, Litovsky S H and Weisman R B 2004 Near-infrared fluorescence microscopy of single-walled carbon nanotubes in phagocytic cells *J. Am. Chem. Soc.* **126** 15638–9

[32] Bianco A, Hoebeke J, Godefroy S, Chaioin O, Pantarotto D and Briand J P 2005 Cationic carbon nanotubes bind to CpG oligodeoxynucleotides and enhance their immunostimulatory properties *J. Am. Chem. Soc.* **127** 58–9

[33] Zanello L P, Zhao B, Hu H and Haddon R C 2006 Bone cell proliferation on carbon nanotubes *Nano Lett.* **6** 562–7
[34] Hu H, Ni Y, Montana V, Haddon R C and Parpura V 2004 Chemically functionalized carbon nanotubes as substrates for neuronal growth *Nano Lett.* **4** 507–11
[35] Chen X, Tam U C, Czlapinski J L, Lee G S, Rabuka D and Zettl A 2006 Interfacing carbon nanotubes with living cells *J. Am. Chem. Soc.* **128** 6292–3
[36] Hu H, Ni Y, Mandal S K, Montana V, Zhao B and Haddon R C 2005 Polyethyleneimine functionalized single-walled carbon nanotubes as a substrate for neuronal growth *J. Phys. Chem.* B **109** 4285–9
[37] Kakudo N, Shimotsuma A, Miyake S, Kushida S and Kusumoto K 2008 Bone tissue engineering using human adipose-derived stem cells and honeycomb collagen scaffold *J. Biomed. Mater. Res.* **84A** 191–7
[38] Li H Y, Zhai W Y and Chang J 2008 *In vitro* biocompatibility assessment of PHBV/Wollastonite composites *J. Mater. Sci. Mater. Med.* **19** 67–73
[39] Bai H and Wang Z Z 2008 Directing human embryonic stem cells to generate vascular progenitor cells *Gene Therapy* **15** 89–95
[40] Gosain A K, Riordan P A, Song L S, Amarante M T, Kalantarian B, Nagy P G, Wilson C R, Toth J M and McIntyre B L 2004 A 1-year study of osteoinduction in hydroxyapatite-derived biomaterials in an adult sheep model: II. Bioengineering implants to optimize bone replacement in reconstruction of cranial defects *Plast. Reconstr. Surg.* **114** 1155–63
[41] Park J W, Suh J Y and Chung H J 2008 Effects of calcium ion incorporation on osteoblast gene expression in MC3T3-E1 cells cultured on microstructured titanium surfaces *J. Biomed. Mater. Res.* **86A** 117–26
[42] Li X M, Feng Q L and Cui F Z 2006 *In vitro* degradation of porous nano-hydroxyapatite/collagen/PLLA scaffold reinforced by chitin fibres *Mater. Sci. Eng.* C **26** 716–20
[43] Fujibayashi S, Neo M, Kim H M, Kokubo T and Nakamura T 2004 Osteoinduction of porous bioactive titanium metal *Biomaterials* **25** 443–50
[44] Popat K C, Chatvanichkul K I, Barnes G L, Latempa T J, Grimes C A and Desai T A 2007 Osteogenic differentiation of marrow stromal cells cultured on nanoporous alumina surfaces *J. Biomed. Mater. Res.* **80A** 955–64
[45] Yim E K F, Pang S W and Leong K W 2007 Synthetic nanostructures inducing differentiation of human mesenchymal stem cells into neuronal lineage *Exp. Cell Res.* **313** 1820–9
[46] Ou K L, Lin C T, Chen S L, Huang C F, Cheng H C, Yeh Y M and Lin K H 2008 Effect of multi-nano-titania film on proliferation and differentiation of mouse fibroblast cell on titanium *J. Electrochem. Soc.* **155** E79–84
[47] Ratner B D, Johnston A B and Lenk T S 1987 Biomaterials surfaces *J. Biomed. Mater. Res.* **21(A1)** 59–90
[48] Zreiqat H, Standard O C, Gengenbach T, Steele J and Howlett C R 1996 The role of surface characteristics in the initial adhesion of human bone-derived cells on ceramics *Cell Mater.* **6** 45–6
[49] Abrams G A, Goodman S L, Nealey P F, Franco M and Murphy C J 2000 Nanoscale topography of the basement membrane underlying the corneal epithelium of the rhesus macaque *Cell Tissue Res.* **299** 39–46
[50] Kumazawa R, Watari F, Takashi N, Tanimura Y, Uo M and Totsuka Y 2002 Effects of Ti ions and particles on neutrophil function and morphology *Biomaterials* **23** 3757–64
[51] Havill L M, Rogers J, Cox L A and Mahaney M C 2006 QTL with pleiotropic effects on serum levels of bone-specific alkaline phosphatase and osteocalcin maps to the baboon ortholog of human chromosome 6p23–21.3 *J. Bone Miner. Res.* **21** 1888–96
[52] Smink J J, Begay V and Leutz A 2005 CCAAT/enhancer binding protein (C/EBP) beta is involved in bone formation *Bone* **36** S269
[53] Lian J B and Stein G S 1996 *Osteoblast Biology* ed R Marcus, D Feldman and J Kelsey (San Diego: Academic)
[54] Ducy P and Karsenty G 1998 Genetic control of cell differentiation in the skeleton *Curr. Opin. Cell Biol.* **10** 614–9
[55] Boskey A L, Gadaleta S, Gundberg C, Doty S B, Ducy P and Karsenty G 1998 Fourier transform infrared microspectroscopic analysis of bones of osteocalcin-deficient mice provides insight into the function of osteocalcin *Bone* **23** 187–96
[56] Ayukawa Y, Takeshita F, Inoue T, Yoshinari M, Shimono M, Suetsugu T and Tanaka T 1998 An immunoelectron microscopic localization of noncollagenous bone proteins (osteocalcin and osteopontin) at the bone-titanium interface of rat tibiae *J. Biomed. Mater. Res.* **41** 111–9
[57] Termine J D, Kleinman H K, Whitson S W, Conn K M, McGarvey M L and Martin G R 1981 Osteonectin, a bone-specific protein linking mineral to collagen *Cell* **26** 99–105
[58] Kilpadi K L, Sawyer A A, Prince C W, Chang P L and Bellis S L 2003 Primary human marrow stromal cells and SaOs-2 osteosarcoma cells use different mechanisms to adhere to hydroxylapatite *J. Biomed. Mater. Res.* **68A** 273–85
[59] Kondo N *et al* 2006 Osteoinduction with highly purified beta-tricalcium phosphate in dog dorsal muscles and the proliferation of osteoclasts before heterotopic bone formation *Biomaterials* **27** 4419–27
[60] Yamasaki H and Sakai H 1992 Osteogenic response to porous hydroxyapatite ceramics under the skin of dogs *Biomaterials* **13** 308–12
[61] Ripamonti U, Van den Heever B and Van Wyk J 1993 Expression of the osteogenic phenotype in porous hydroxyapatite implanted extraskeletally in Baboons *Matrix* **13** 491–502
[62] Magan A and Ripamonti U 1996 Geometry of porous hydroxyapatite implants influences osteogenesis in baboons (*Papio Ursinus*) *J. Craniofac. Surg.* **7** 71–8
[63] Hing K A 2005 Bioceramic bone graft substitutes: influence of porosity and chemistry *Int. J. Appl. Ceram. Technol.* **2** 184–99

Journal of
Nanoscience and Nanotechnology
Vol. 6, 1649–1654, 2006

Preparation and Characterization of Polypeptide-Stabilized Gold Nanoparticles

Tetsu Yonezawa[1, 2, *], Takashi Nomura[2], Takatoshi Kinoshita[3], and Kunihito Koumoto[2]

[1] *Department of Chemistry, Graduate School of Science, The University of Tokyo, Hongo, Bunkyo-ku, Tokyo 113-0033, Japan*
[2] *Department of Applied Chemistry, Graduate School of Engineering, Nagoya University, Furo-cho, Chikusa-ku, Nagoya 464-8503, Japan*
[3] *Department of Material Science, Graduate School of Engineering, Nagoya Institute of Technology, Gokiso-cho, Showa-ku, Nagoya 466-8555, Japan*

Helical polypeptides have a highly rigid conformation. In order to control self-assembling structure in nanoscale, the rigidity of the stabilizing molecules, which is working as scaffolds, is highly important. Furthermore, the molecular lengths of polypeptides can be readily controlled by using their unique polymerization methods. In this study, we have used helical polypeptides as the stabilizing reagent of metal nanoparticles. As for rigid helical polypeptides, poly(γ-benzyl-L-glutamate) (PBLG) was selected, and was synthesized by *N*-carboxylic acid anhydride (NCA) polymerization. Preparation of helical polypeptide-stabilized gold nanoparticles using a two-phase reduction process from the corresponding metal salts with $NaBH_4$ is therefore introduced. PBLG itself did not have good stabilizing ability for metal nanoparticles and a terminal attaching ligand was indispensable for nanoparticle stabilization and, for this purpose, lipoic acid was selected. It is estimated that lipoic acid functionalized polypeptide molecules were attached perpendicularly to the particle surface by lipoic acid group. The size and structure, as well as assembling will be discussed in this manuscript.

Keywords: Gold, Nanoparticle, Polypeptide, Monolayer, Scaffold.

1. INTRODUCTION

At the nanometer scale, chemistry and physics of matter bridge between those of bulk materials and atoms or molecules.[1–4] Nanoparticle research has been expanded enormously from the viewpoint of specific properties according to the size of the particles. In order to develop building blocks for nanomaterial devices, controlling the organic stabilizing shell surrounding the nanoparticles is an important technology.[5] In order to control the organic shell thickness, the rigidity of the stabilizer molecules and their lengths is extremely important. We have used a fluorocarbon thiol, which has a rigid conformation, as the stabilizing reagent of nanoparticles, and they assembled highly uniformly in a wide area by simple casting of the dispersion onto a TEM grid.[6] Helical macromolecules can be very useful for this purpose because such molecules have a rigid conformation. On the other hand, controlled macromolecules such as dendrimers as well as some kind of proteins have been also used as effective controlled shells for nanoparticle assemblies.

On the other hand, some kinds of biopolymers can be readily synthesized with a uniform molecular weight and a uniform structure. For example, controlled DNA molecules can be readily obtained by using the PCR (polymerase chain reaction) method. Polypeptide molecules with controlled arrangement amino acids can be obtained using artificial genes and colon bacilli. For controlling the thickness and functions of organic shell molecules, using such biopolymers can be useful. Recently, during our preparation of this manuscript, another group has reported the preparation of polypeptide-stabilized gold nanoparticles.[7] They have chosen asymmetric disulfide moiety for the attachment of the polypeptide compounds onto the nanoparticle surface.

We would like to introduce, in this study, an easier preparation process, using a DL-lipoic acid for the ligand moiety, which is commercially available. As for the polypeptide, poly(γ-benzyl-L-glutamate) (PBLG) has been selected. Lipoic acid-terminated helical polypeptides (PBLGLipo) can be adsorbed on gold surfaces densely with a small tilt angle.[8] We compared the structure and the assembling feature of the polypeptide-stabilized gold

*Author to whom correspondence should be addressed.

 1533-4880/2006/6/1649/006 doi:10.1166/jnn.2006.222

nanoparticles with the lipoic acid-stabilized ones. We will also discuss the detailed structure of the PBLGLipo-stabilized gold nanoparticles briefly.

2. EXPERIMENTAL DETAILS

2.1. Materials

Water was purified by a Milli-Q system (>18 MΩ). Reagents were used as received without further purification. As the metal sauce, $HAuCl_4$ $4H_2O$ (Nakarai Tesque, GR grade) was used. DL-lipoic acid is racemic (Tokyo Kasei).

2.2. Preparation of Lipoic Acid-Terminated Helical Polypeptide

Poly(γ-benzyl-L-glutamate) (PBLG) was synthesized by NCA (*N*-carboxylic acid anhydride) method.[9,10] γ-Benzyl-L-glutamate (BLG, 5 g) was introduced into a 500 cm^3 three neck-round bottom flask. Dry tetrahydrofuran (THF, 250 cm^3) was introduced into the flask as the solvent. After N_2 bubbling (60 min), triphosgen (2.52 g) was introduced into this reaction flask. The turbid dispersion was changed into clear. After filtering over a G5 glass filter in order to separate the precipitates, the obtained solution was pored into a 500 cm^3 round bottom flask. After evaporation of the solvent to 50 cm^3, excess dried *n*-hexane was added into the flask to precipitate BLG-NCA (Scheme 1). After collecting by filtration, BLG-NCA was washed with *n*-hexane carefully and dried *in vacuo*. Then, the obtained BLG-NCA (1 g) was introduced into dried DMF (smallest amount) and *n*-hexylamine (10.4×10^{-3} cm^3) was added dropwise under intensive stirring. After 3 days, this reaction mixture was injected dropwise into diethyl ether (150 cm^3) in order to re-precipitate

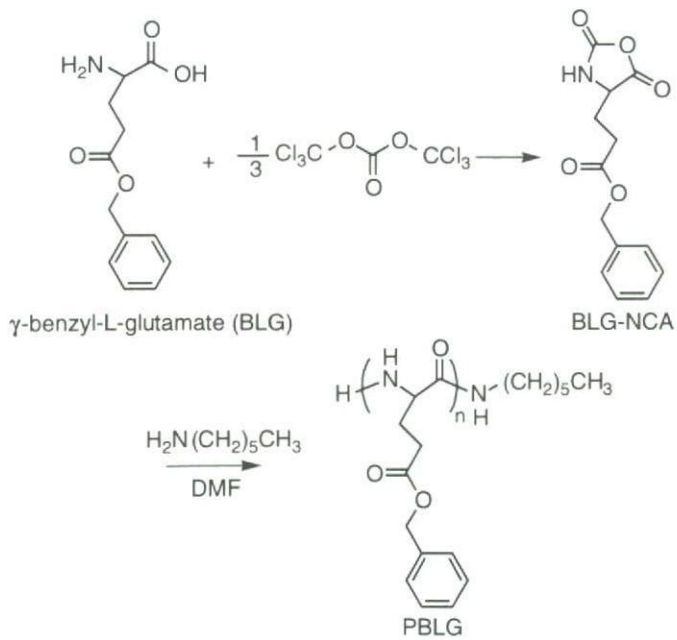

Scheme 1.

PBLG (see also Scheme 1). Again filtration over G5 glass filter, the product was collected.

Preparation of PBLGLipo (PBLG + lipoic acid; PBLG containing stabilizing reagent) was carried out by amide formation with PBLG and DL-lipoic acid by using DCC (dicylohexylcarbodiimide) as a dehydrate reagent (Scheme 2). DCC (100 mg), DL-lipoic acid (100 mg), 1-hydroxybenzotriazole (HOBt, 65.4 mg) were injected into 1.5 cm^3 of dichloromethane and stirred for a few hours. In another vial, PBLG (300 mg) was dissolved into 1 cm^3 of dichloromethane. These two solutions were mixed together and were kept stirring for 12 h. Ethanol was dropped into this flask to re-precipitate the product. The product was washed carefully by ethanol.

2.3. Preparation of Gold Nanoparticles

Preparation of gold nanoparticles was carried out by two-phase method for PBLGLipo-stabilized nanoparticles[11] and by one-phase method for lipoic acid-stabilized nanoparticles.[12] The reducing reagent was $NaBH_4$.

PBLGLipo-stabilized gold nanoparticles were obtained in dichloromethane/water. PBLGLipo could be resolved into dichloromethane. Into a 100-cm^3 round bottom flask, 10 cm^3 of water and 10 cm^3 of dichloromethane were introduced. Into this mixed solvent, $HAuCl_4$ and PBLG-Lipo was introduced at the same concentration ([Au] = [PBLGLipo] = 2.0×10^{-4} mol dm^{-3}). As phase transfer reagent, tetra-*n*-octylammonium bromide (TOAB) was introduced ([TOAB] = 8.0×10^{-4} mol dm^{-3}). After stirring this mixed solution, the color of the dichloromethane phase turned into orange. Then, aqueous $NaBH_4$ (2.0×10^{-3} mol dm^{-3}, 5 cm^3) was added dropwise and the solution was kept stirring for 1 day.

Lipoic acid-stabilized gold nanoparticles were also prepared for comparison. In this case, one aqueous phase method was used. Representative preparation process was as follows. Into a 100-cm^3 round bottom flask, designed amount of DL-lipoic acid and $HAuCl_4$ aqueous solution was added. Then, 5 cm^3 of aqueous $NaBH_4$ (4.0×10^{-1} mol dm^{-3}) was added dropwise. The dispersion was instantly turned into black, which informed us the formation of gold nanoparticles. The dispersion was kept stirring for 3 h.

2.4. Characterization

Transmission electron microscopy (TEM, Hitachi H-800, acceleration voltage = 200 kV) was used for observing the size of the obtained nanoparticles and their assembling structures. The samples were prepared by dropping the nanoparticle dispersions onto carbon thin film covered copper grids. FT-IR with a Perkin Elmer 2000 was observed in order to check the completion of polymerization. The polymerization degree of the obtained polypeptide was determined from ^1H NMR obtained with a JEOL

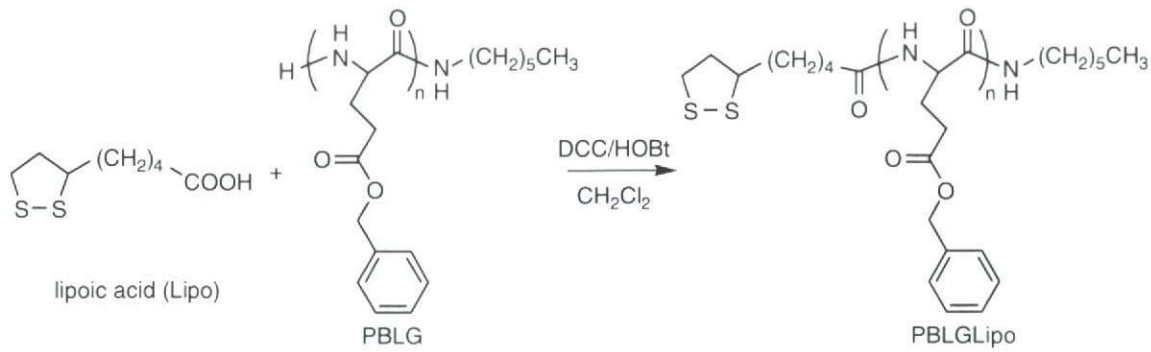

Scheme 2.

JNM-GX400. UV-Vis spectra were obtained with a JASCO V-550.

3. RESULTS AND DISCUSSION

3.1. Synthesis of Functionalized Polypeptides

Synthesis of PBLG has been successfully carried out by an NCA process. We have used excess triphosgen in order to obtain polypeptide molecules with a longer chain. The average polymerization numbers, calculated from the ^{1}H NMR spectra, however, were relatively low as 38.3 and 17.1. The diameter of PBLG is 1.4 nm and their lengths can be calculated as 5.8 nm and 2.6 nm, respectively. It is probably due to the low reaction ratio with our reaction process. Probably, a longer reaction time or repeat of NCA reaction should be used. The error of the distributions of PBLG can be estimated as ca. 20%. Clear molecular weight distributions were not obtained. Hereafter, we call these two polypeptides as $PBLG_{38}$ and $PBLG_{17}$, respectively.

In this study, we have selected DL-lipoic acid as the coordinating group of the stabilizing polypeptides. DL-Lipoic acid is a food additive, non-toxic, and has high commercial availability. Preparation of PBLGLipo was carried out by amidation using DCC as a condensation reagent. The obtained product was washed by ethanol. The reaction time was 24 h. First we have tried to functionalize $PBLG_{38}$. ^{1}H NMR spectrum of the product revealed that only 43.3% of $PBLG_{38}$ was terminated by lipoic acid. According to the rigid secondary conformation of PBLG, hydration could not proceed rapidly. Purification of $PBLG_{38}$Lipo was essayed by repeated reprecipitation, but in vain. Moreover, the condensation of $PBLG_{38}$ and Lipo was very slow and repeated condensation could not give a very high purity of $PBLG_{38}$Lipo. Lipoic acid group is too small compare to $PBLG_{38}$ and the pure product could not be obtained. Therefore, we have used this crude compounds (43.3% $PBLG_{38}$Lipo and 56.7% $PBLG_{38}$) for nanoparticle preparation. Free $PBLG_{38}$ may affect the structure of obtained nanoparticles because PBLG has a rigid rod-type shape and easily self-assembled. However, as described above, $PBLG_{38}$ itself did not have stabilizing ability and the concentration of $PBLG_{38}$ at the preparative condition is not so high to form a strong self-assembled structure. And the obtained nanoparticles have spherical forms as shown in the TEM picture as shown below (Fig. 3a). Therefore, we have concluded that no considerable effect of free $PBLG_{38}$ molecules can be observed on nanoparticle formation.

In order to obtain pure PBLGLipo, higher reaction ratio of amidation between PBLG and Lipo is indispensable. For this purpose,

(1) higher reaction temperature,
(2) longer reaction time, and/or
(3) repeated reaction are needed.

Then, we repeated amidation with lipoic acid and $PBLG_{17}$. Every time, we added lipoic acid, DCC, and HOBt into the flask. But these reagents can be separated by washing out with ethanol. In order to reveal the reaction rate of this amidation, the peak intensity of UV-Vis spectra at 335 nm was observed. This peak can be attributed to lipoic acid. After three times of amidation, the reaction rate became 100%. Probably, this repeated reaction with large excess lipoic acid is the key to complete this amidation. We have also used $PBLG_{17}$Lipo as the stabilizing reagent of gold nanoparticles.

3.2. Preparation and Characterization of Gold Nanoparticles

First we have essayed to prepare PBLG-stabilized gold nanoparticles. As PBLG is hydrophobic, it may be adsorbed onto particle surface. If the adsorption is enough strong, the particles can be dispersed. The preparation was carried out by two-phase process. In this two-phase preparation, tetra-*n*-octylammonium bromide (TOAB) was used as the phase-transfer reagent of $AuCl_4^-$. As shown in the TEM picture in Figure 1, some small nanoparticles could be observed. Probably they were stabilized by TOAB as other researchers have reported.[13] However, in this dispersion, large aggregates were also observed at the center of Figure 1. This phenomenon probably induced by PBLG, which has a helical rigid secondary structure.

We have also prepared lipoic acid-stabilized gold nanoparticles. Lipoic acid has a disulfide group, and this

Fig. 1. TEM image of gold nanoparticles prepared by two-phase $NaBH_4$-reduction method in the presence of PBLG.

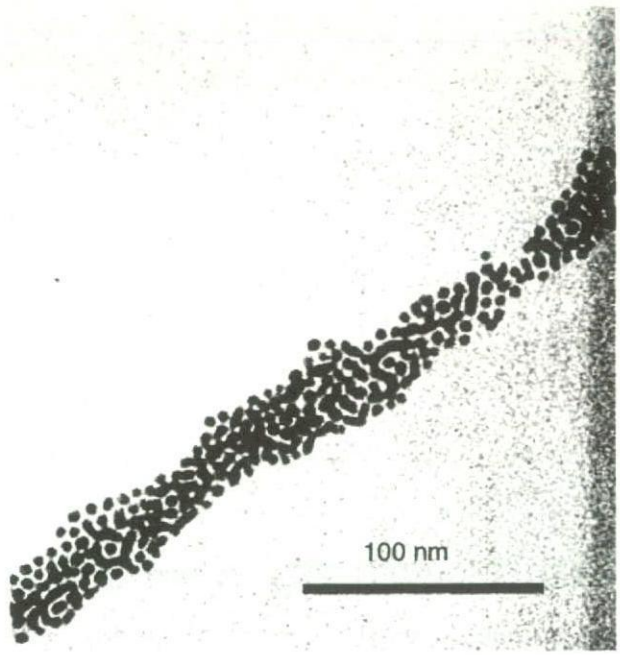

Fig. 2. TEM image of lipoic acid-stabilized gold nanoparticles prepared by one-phase $NaBH_4$-reduction method.

group can attach to the gold surface. Furthermore, $NaBH_4$, which is used as the reducing reagent of $HAuCl_4$ to Au, can also reduce disulfide to two thiols (–S–S– → –SH + –SH), which can strongly coordinate to Au. A large excess amount of $NaBH_4$ was added to the $HAuCl_4$ and PBLGLipo mixed solutions. Therefore, this reduction of disulfides can be proceeded in these solutions during the preparation even the reaction rates of $Au^{3+} \rightarrow$ Au and –S–S– → –SH + –SH are very different. We have tried 4 entries with various concentrations of lipoic acid and $HAuCl_4$, which was collected in Table I. In all cases, dark black dispersions were obtained which indicated that the reduction of $HAuCl_4$ was completed. However, when the concentration of lipoic acid was lower, the stability of gold nanoparticles was not enough to be stably dispersed. During this reduction process, the solution was alkaline because a large excess of $NaBH_4$ was introduced. Therefore, lipoic acid should have become sodium lipoate. Because of the charge repulsion between lipoate molecules on the surface of the nanoparticles, large excess lipoic acid is indispensable for the preparation of gold nanoparticles. Similar phenomena were also observed during the preparation of thiocholine bromide stabilized gold nanoparticles.[14]

Table I. Preparation of lipoic acid-stabilized gold nanoparticles at various concentration of lipoic acid and $HAuCl_4$.

Entry	[Lipoic acid]/mol dm^{-3}	[$HAuCl_4$]/mol dm^{-3}	Nanoparticle[a]
1	2.5×10^{-4}	5.0×10^{-3}	−
2	5.0×10^{-4}	5.0×10^{-3}	−
3	5.0×10^{-3}	5.0×10^{-3}	+
4	5.0×10^{-3}	1.0×10^{-2}	+

[a]+: Stable nanoparticle dispersion was obtained. No aggregation or precipitation was observed. −: Nanoparticle dispersion was obtained. However, precipitates were generated.

Size dispersion of lipoic acid-stabilized gold nanoparticles is relatively wide and the average diameter is 4.0 nm. Careful observation on the TEM picture (Fig. 2) reveals that some fusion of the gold nanoparticles occurs on the TEM grid. Usually, thiol-stabilized gold nanoparticles have a spherical form. However, in this picture, many particles are spherical but some peanut-like or worm-type semi-continuous structures can be observed. Usually, this type of preparation of gold nanoparticles does not give such semi-continuous structures. Division of materials into nano-dimension, their melting temperature usually becomes lower. However, the melting temperature of gold at 4 nm is ca. 900 K (630 °C).[15] Therefore, melt of the particles did not occur on the TEM grid. But in our and other group's previous studies,[14, 16, 17] densely located gold nanoparticles on a substrate with very small interparticle distance showed self-fusion of gold nanoparticles at a much lower temperature than the melting point. This is probably due to the atomic motion on the surface of gold.

PBLGLipo-stabilized gold nanoparticles were prepared by using two-phase method. When we use $PBLG_{38}Lipo$ as the stabilizer, we used the concentration of crude $PBLG_{38}Lipo$ at [crude $PBLG_{38}Lipo$] $= 4.62 \times 10^{-4}$ mol dm^{-3} because the reaction ratio was 43.3% ($1/0.433 \times 2.0 = 4.62$). The obtained dispersion was very stable and no aggregation or precipitation was observed for weeks. No obvious aggregates were found. Therefore, the nanoparticles were stabilized by PBLGLipo but not by non reacted PBLG. Purification of $PBLG_{38}Lipo$ was tried intensively but in vain in our case. Therefore, as described above, we repeated amidation between PBLG and Lipo in the case of $PBLG_{17}Lipo$ in order to obtain a pure PBLGLipo. In order to separate $PBLG_{38}Lipo$-stabilized gold nanoparticles

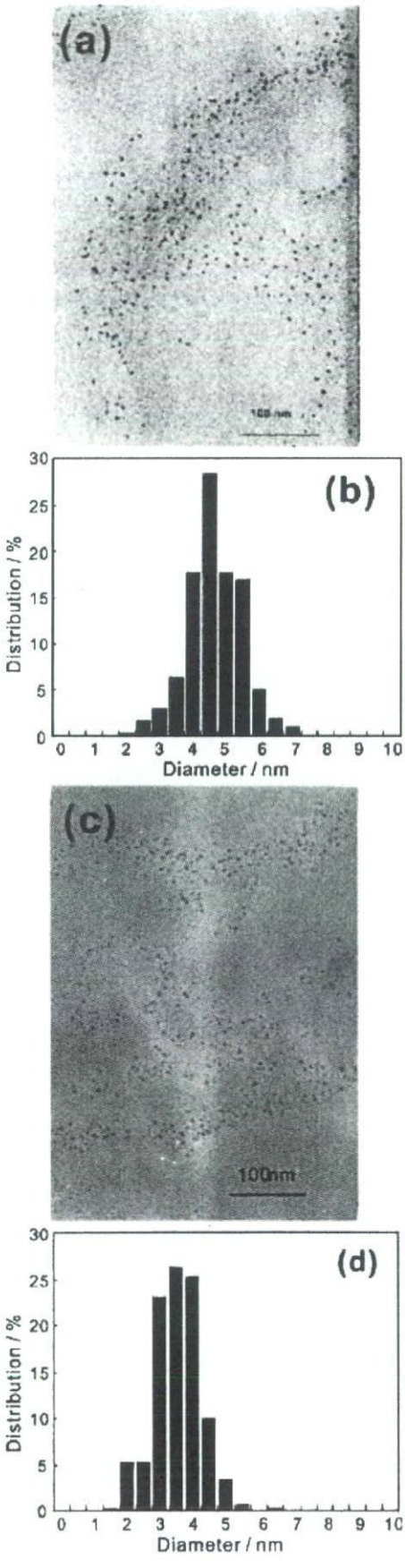

Fig. 3. TEM images of (a) $PBLG_{38}$Lipo-stabilized gold nanoparticles and (c) $PBLG_{17}$Lipo-stabilized gold nanoparticles. Size distributions of (b) $PBLG_{38}$Lipo-stabilized gold nanoparticles and (d) $PBLG_{17}$Lipo-stabilized gold nanoparticles obtained from Figures 3a and 3c, respectively.

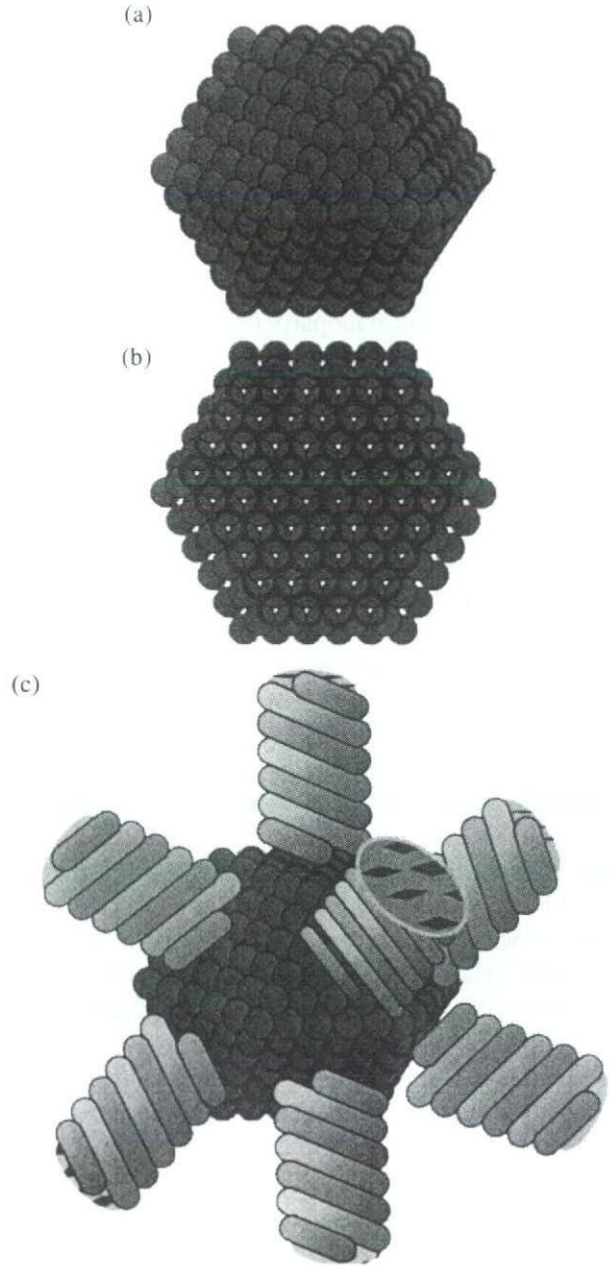

Fig. 4. Schematic figure of stabilizing structure of $PBLG_{17}$Lipo-stabilized gold nanoparticle. (a) Illustration of the metal core of 3.3-nm gold nanoparticle (Au_{561}), (b) cross-sectional image of the metal core: Au_{561}, 5-shell structure, (c) stabilization structure of $PBLG_{17}$Lipo-stabilized gold nanoparticle.

and unbounded $PBLG_{38}$Lipo, repeated ultracentrifugation (Hitachi GX-150) was used (50 000 rpm for 1 h). Figure 3a shows the TEM image of $PBLG_{38}$Lipo-stabilized gold nanoparticles. The average diameter of these nanoparticles is 4.4 nm. In this TEM image, the gold nanoparticles are observed separately with long inter-particle distance. No fusion of the nanoparticles can be observed. However, unfortunately well-ordered assembly of $PBLG_{38}$Lipo-stabilized gold nanoparticles was observed in the TEM image probably because of too low concentration of gold nanoparticles in the dispersion.

$PBLG_{17}$Lipo-stabilized gold nanoparticles were prepared in the same manner. The TEM image of the obtained

gold nanoparticles is shown in Figure 3c. The average diameter is 3.3 nm which is slightly smaller than $PBLG_{38}$Lipo-stabilized ones. No fusion of the nanoparticles can be observed in this image either. Higashi reported also the size of nanoparticles can be varied with the length of polypeptide.[7] Braun also reported that the molecular weight of thiol-terminated polymer affect the particle sizes.[18] First of all, bulky thiol compounds may give smaller nanoparticles,[19] therefore, this PBLGLipo system could give such small nanoparticles in the both cases due to its bulkyness of helix structure. However, the longer PBLG has a stronger intermolecular interaction and self-assemble property.[20] This property can prevent an effective coordination of $PBLG_{38}$Lipo onto gold nanoparticles and it may give a larger nanoparticles.

In order to understand the stabilizing structure of PBLGLipo on gold nanoparticles, we have estimate the particle structure. As the average size of $PBLG_{17}$Lipo-stabilized gold nanoparticles is 3.3 nm, the cross-sectional image of the gold core can be estimated as shown in Figure 4a. The radius of Au atom is 0.134 nm. Therefore, these nanoparticles have the 5- or 6-shell structure model with 11 or 13 gold atoms at the longest axis. Each nanoparticle of a 5-shell or 6-shell model contains 561 or 923 gold atoms, respectively (each shell has $10\ n^2 + 1$ atoms (n = shellnumber)). The smaller 5-shell particle is consisted of 6 squares with the side length of 1.8 nm, and 6 triangles with the side length of 1.8 nm. Here, we adapt the Higashi's result that showed PBLG forms helical structures even on the gold nanoparticles. As the diameter of the helix of PBLG is 1.4 nm, only one $PBLG_{17}$Lipo should be attached to each square surface or triangle surface. Therefore, the stabilizing structure of $PBLG_{17}$Lipo-stabilized gold nanoparticle can be estimated as shown in Figure 4c (a representative smaller 5-shell model).

4. CONCLUSION

This manuscript has described the preparation of lipoic acid functionalized poly(γ-benzyl-L-glutamate) (PBLG-Lipo)-stabilized gold nanoparticles and discussed the preparation and the structure. Repeat amidation with lipoic acid and PBLG was needed to obtain pure PBLGLipo. The size of gold nanoparticles was varied with the molecular length. The stabilizing structure was estimated from the size of the nanoparticles and PBLGLipo possessing a helical structure on the particle surface.

Acknowledgments: The financial support by Ogasawara Foundation is gratefully acknowledged. Authors thank M. Hattori for his experimental assistance. T. K. thanks Japan Aerospace Exploration Agency (JAXA) for its partial financial support.

References and Notes

1. T. Yonezawa and N. Toshima, *New J. Chem.* 1179 (**1998**).
2. G. Schmid (ed)., *Nanoparticles*, Wiley-VCH, Weinheim (**2004**).
3. T. Yonezawa, Well-Dispersed Bimetallic Nanoparticles. In *Morphology Control of Materials and Nanoparticles*, edited by Y. Waseda and A. Muramatsu, Springer, Berlin (**2004**), p. 85.
4. M.-C. Daniel and D. Astruc, *Chem. Rev.* 104, 293 (**2004**).
5. R. Shenhar and V. M. Rottello, *Acc. Chem. Res.* 36, 549 (**2003**).
6. T. Yonezawa, S. Onoue, and N. Kimizuka, *Adv. Mater.* 13, 140 (**2001**).
7. N. Higashi, J. Kawahara, and M. Niwa, *J. Colloid Interf. Sci.* 288, 83 (**2005**).
8. Y. Miura, S. Kimura, Y. Imanishi, and J. Umemura, *Langmuir* 14, 6935 (**1998**).
9. C. H. Bamford, A. Elliott, and W. E. Handy, Synthetic Polypeptides, Academic Press, New York (**1959**).
10. T. Kinoshita, S. Hayashi, and Y. Yokogawa, *J. Photochem. Photobiol. A* 145, 101 (**2001**).
11. M. Brust, M. Walker, D. Bethell, D. J. Schiffrin, and R. Whyman, *J. Chem. Soc., Chem. Commun.* 801 (**1994**).
12. M. Brust, J. Fink, D. Bethell, D. J. Schiffrin, and C. Kiely, *J. Chem. Soc., Chem. Commun.* 9464 (**1995**).
13. J. Fink, C. J. Kiely, D. Bethell, and D. J. Schiffrin, *Chem. Mater.* 10, 922 (**1998**).
14. T. Yonezawa, S. Onoue, and N. Kimizuka, *Chem. Lett.* 1172 (**2002**).
15. Ph. Buffat and J.-P. Borel, *Phys. Rev. A* 13, 2287 (**1976**).
16. T. Yonezawa, S. Onoue, and N. Kimizuka, *Chem. Lett.* 34, 1498 (**2005**).
17. C. J. Kiely, J. Fink, M. Brust, D. Bethell, and D. J. Schiffrin, *Nature* 396, 444 (**1998**).
18. R. G. Shimmin, A. B. Schoch, and P. V. Braun, *Langmuir* 20, 5613 (**2004**).
19. T. Yonezawa, K. Yasui, and N. Kimizuka, *Langmuir* 17, 271 (**2001**).
20. H. Niwa, M. Morikawa, and N. Higashi, *Angew. Chem. Int. Ed.* 39, 960 (**2000**).

Received: 27 August 2005. Accepted: 4 October 2005.

Fullerenes, Nanotubes, and Carbon Nanostructures, 15: 303–309, 2007

ISSN 1536-383X print/1536-4046 online
DOI: 10.1080/15363830701423773

Taylor & Francis
Taylor & Francis Group

The Purity and Thermal Stability in Air of Metal-Encapsulating Carbon Nanocapsules (MECNCs)

Motohiro Uo, Hanako Kachi, Tsukasa Akasaka, and Fumio Watari

Department of Biomedical Materials and Engineering, Graduate School of Dentistry, Hokkaido University, Sapporo, Japan

Yoshinori Sato, Kenichi Motomiya, and Kazuyuki Tohji

Graduate School of Environmental Studies, Tohoku University, Sendai, Japan

Abstract: Rare earth elements (Y, La, Ce, Nd, Gd and Dy) encapsulated by carbon nanocapsules (CNCs) were synthesized and their purity and air oxidation stability were estimated. The purity was estimated as the rare earth carbide content. Gd- and Dy-encapsulating CNCs had higher than 30 wt% and others 15 to 20 wt%. Encapsulated rare earth carbide was oxidized by heating in air at 400°C or higher. This suggested oxidation damage to the graphene capsules of CNCs.

Keywords: Metal encapsulating carbon nanocapsules, rare earth, carbide, purity, thermal stability

INTRODUCTION

Metal-encapsulating carbon nanocapsules (MECNCs) are several tens of nanometers in diameter and consist of a graphene sheet structure encapsulating a metallic carbide. MECNCs have a surface covered by a graphene sheet, so they have quite high chemical stability (1–10). In the capsule synthesized

Received 19 September 2006, Accepted 15 December 2006
Address correspondence to Motohiro Uo, Department of Biomedical Materials and Engineering, Graduate School of Dentistry, Hokkaido University, 060-8586 Sapporo, Japan. E-mail: uo@den.hokudai.ac.jp

by using a direct current arc-discharge method with a lanthanide-loading graphite anode, lanthanide is usually encapsulated as a carbide. The formation of MECNCs was suggested as the segregation of excess carbon composition from the metal carbide droplets while they are cooling (4). Metallofullerenes have been studied as contrast agents in X-ray or magnetic resonance imaging (11, 12).

MECNCs also contain metallic elements in the graphite capsule, but the size of the capsule and the amount of encapsulated metallic elements are a hundred times larger than metallofullerenes. In addition, the graphene capsules have high chemical stability and the encapsulated metals are stable in air, water and concentrated sulfuric acid, and these features will provide higher imaging and tracing efficiencies as contrast agents or tracers as the authors have reported the low cytotoxicity of MECNCs (13). In the application of MECNCs, their purity and the chemical stability of the graphene capsules must be estimated.

EXPERIMENTAL PROCEDURES

MECNCs were synthesized by a direct current arc-discharge between a pure graphite cathode and a metal-loaded graphite anode in a helium atmosphere. A pure graphite rod (purity 99.9%, Wakomu Denso Co., Japan) and a graphite rod loaded with Y_2O_3, La_2O_3, CeO_2, Nd_2O_3, Gd_2O_3 and Dy_2O_3 powder (99.9%, Wako Pure Chemical Industries, Japan) as the source of rare earth were used as the cathode and anode, respectively. The arc-discharge was carried out in helium gas at 500 Torr. A carbonaceous deposit on the cathode was corrected and the synthesis of the MECNCs was confirmed with TEM observation (TEM: Hitachi, HF-2000, Japan), energy-dispersive X-ray spectroscopy analysis (EDXS: NORAN Instruments, VANTAGE, USA) and X-ray diffraction (XRD: Rigaku, Multiflex, Japan). As-grown MECNCs, MECNCs heated at 350 to 450°C in air for 30 minutes and MECNCs heated at 450°C in vacuum (10^{-6} torr) were subjected to X-ray diffraction to estimate the crystalline state of encapsulated rare earth. Some MECNCs were heated at 800°C for 2 hours to burn out the graphene capsule and the rare earth oxide that remained was weighed. The rare earth carbide contents in as-grown MECNCs were converted from the final oxide weight and the chemical formulae of the rare earth carbides and oxides were assigned.

RESULTS AND DISCUSSION

MECNCs encapsulating Y, La, Ce, Nd, Gd and Dy were successfully synthesized. Later, those MECNCs are abbreviated as Y-CNCs. Figure 1 shows the TEM image of Ce-CNCs. We observed many MECNCs as well as

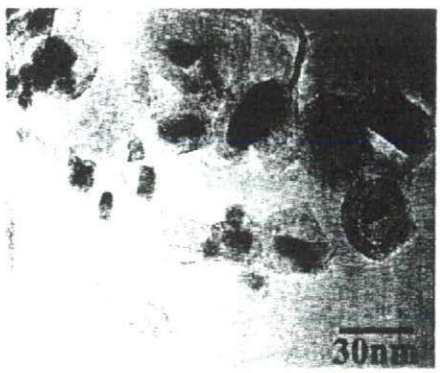

Figure 1. High magnification TEM image of MECNCs (Ce-CNCs).

non-encapsulating carbon nanocapsules. The single-crystal CeC_2 compounds were encapsulated in the multi-walled carbon layers. The fact that the CeC_2 interior was single-crystalline was confirmed by electron diffraction (9) and EDXS. The estimated rare earth carbide contents in various MECNCs are presented in Table 1. The weights of the MECNCs were mostly obtained from the rare earth carbide cores. Therefore, the carbide contents were close to the purity of the MECNCs. The purity levels of Gd- and Dy-containing CNCs were more than 30 wt% and others were less than 20 wt%. Therefore, graphite, amorphous carbon and vacant carbon nanocapsules were contained as impurities.

Figure 2(a) shows the X-ray diffraction spectra of Ce-encapsulating nanocapsules (Ce-CNCs) as grown and heated at 350 to 450°C. As-grown Ce-CNCs show diffraction peaks derived from the graphite and CeC_2. The spectrum was not changed after heating at 350°C, but CeO_2 appeared after heating at higher than 400°C. Rare earth carbides are instable in air and easily oxidized. In MECNCs, however, the graphene capsule is airtight; therefore, the rare earth carbide is isolated from the air. When heated at higher than 400°C in air, the graphene capsule was damaged by oxidation and the encapsulated CeC_2 was oxidized to CeO_2. Similarly, Y-CNCs showed peaks derived from the oxide species (Y_2O_3) after heating at 400°C

Table 1. Rare earth carbide content in raw MECNCs

MECNCs	Chemical formula of encapsulated carbide	Carbide content (wt%)
Y-CNCs	YC_2	16
La-CNCs	LaC_2	19
Ce-CNCs	CeC_2	19
Nd-CNCs	NdC_2	20
Gd-CNCs	GdC_2	35
Dy-CNCs	DyC_2	31

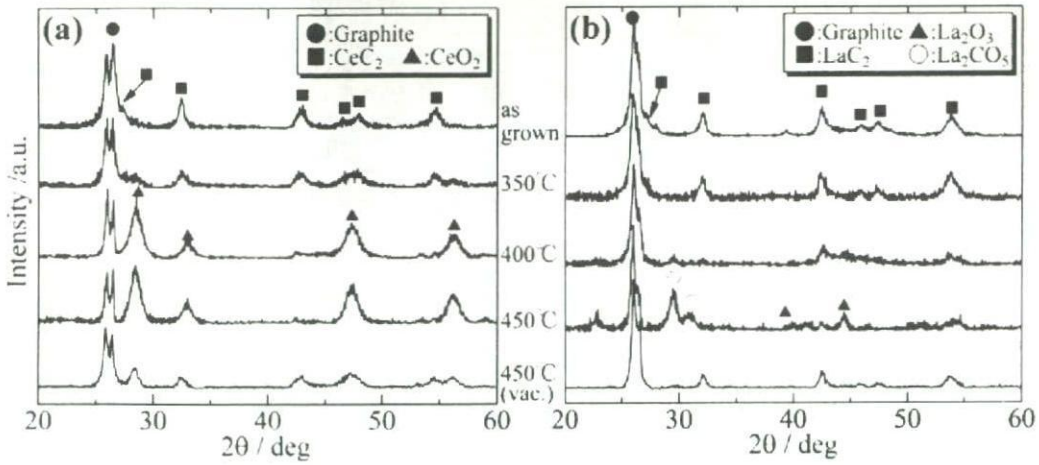

Figure 2. Changes in X-ray diffraction spectra of Ce- and La-CNCs with heat treatment.

or higher. Figure 2(b) shows the X-ray diffraction spectra of La-CNCs as grown and heated at 350 to 450°C. As-grown La-CNCs show diffraction peaks derived from the graphite and LaC_2.

After heating at 400°C, peaks of LaC_2 became weak and peaks of La_2O_3 and La_2CO_5 appeared at above 450°C. Nd-CNCs showed $Nd_2O_2CO_3$ after 450°C. These results showed that La- and Nd-CNCs were stable at lower than 350°C and that carbonate or oxicarbonate species were formed at 450°C. After heating at 450°C in vacuum, Ce-CNCs showed CeO_2 peaks, however, La-CNCs were not changed. Also, Y-CNCs and Nd-CNCs were not changed after heating at 450°C in vacuum. Then, Ce-CNCs would be less stable for heating.

Figure 3(a) shows the X-ray diffraction spectra of Gd-CNCs as grown and heated at 350 to 450°C. The peaks derived from GdC_2 remained after heating at 400°C. At 450°C, peaks assigned to GdC_2 disappeared and unclear peaks

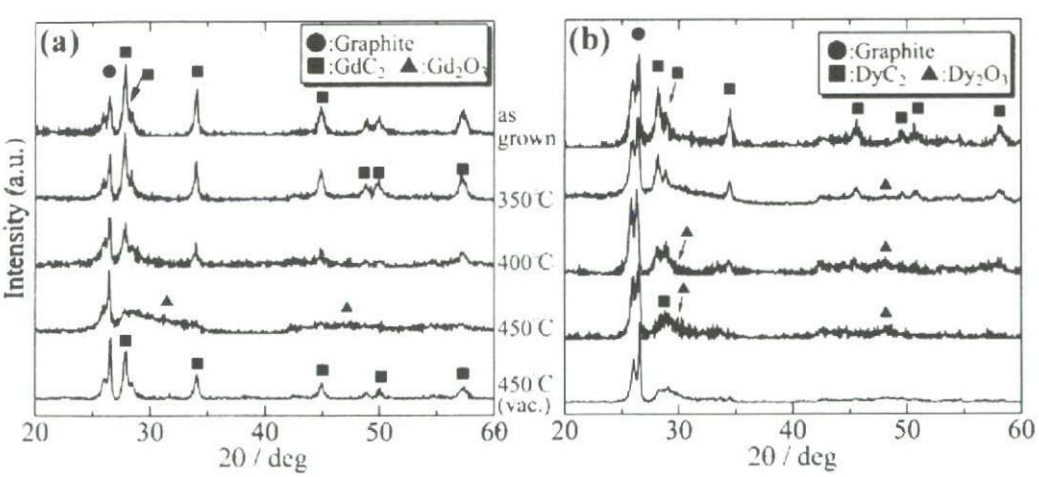

Figure 3. Changes in X-ray diffraction spectra of Dy- and Gd-CNCs with heat treatment.

assigned to Gd_2O_3 were slightly increased. Gd-CNCs was not changed after heated at 450°C in vacuum. As shown in Figure 3(b), the peaks derived from DyC_2 remained after heating at 400°C, but the peaks were broadened. Dy-CNCs after heated at 450°C in vacuum was similar to that after heated in air. Therefore, Gd-CNCs would have the highest stability for heating in air and vacuum.

Figure 4 shows the TEM images of Gd- and Dy-CNCs after heated at 450°C. Gd or Dy encapsulating CNCs (points 1 and 3 in Figure 4) were remained and large granules (points 2 and 4) were generated after heating. The compositions of each point analyzed by EDXS were tabulated in Table 2. Points 1 and 3 contain the rare earth (Gd or Dy) and C. Then, the remaining of Gd-and Dy-CNCs after heated at 450°C could be confirmed. Point 2 and 4 which were generated large granules showed high oxygen content. Those granules could be assumed that the most of MECNCs were oxidized and degraded by heating, and then encapsulated rare earth was formed oxide particles. In Y-, La-, Ce-and Nd-CNCs that showed no carbides in XRD spectra after heated at 450°C, the remained MECNCs could not observed by TEM observation. Therefore, the heating stability estimated by XRD was confirmed by TEM observation.

Oxidation treatment at around 500°C was useful for the purification of carbon nanotubes because the impurities, e.g., amorphous carbon or hydrocarbon, were burned out before nanotube oxidation. In this study, the encapsulated rare earth carbides in MECNCs were oxidized by heating at 400 to 450°C in air. Ajayan et al. suggested that both the strain at the tip and the presence of pentagons might help the initiation of the oxidation at the caps of carbon nanotubes (14).

MECNCs have tips that would contain pentagons, thus, heating in air would promote the oxidation at the tips of the graphene capsules of MECNCs and airtightness is lost. Then the encapsulated rare earth carbide is oxidized. The airtightness of the graphene capsule means that the

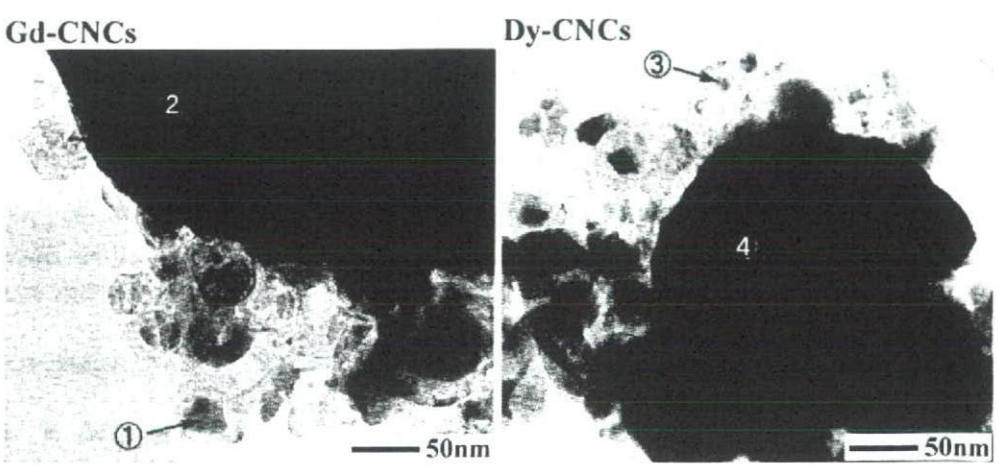

Figure 4. TEM images of Dy- and Gd-CNCs after heat treatment at 450°C.